Resolving Single-Molecule Assembled Patterns with Superresolution Blink-Microscopy

ARTICLE *in* NANO LETTERS · DECEMBER 2009

Impact Factor: 13.59 · DOI: 10.1021/nl903730r · Source: PubMed

10 AUTHORS, INCLUDING:

Christian Steinhauer
Technische Universität Braunschweig
24 PUBLICATIONS **1,194** CITATIONS
SEE PROFILE

Elias M Puchner
University of Minnesota Twin Cities
28 PUBLICATIONS **929** CITATIONS
SEE PROFILE

Jan Vogelsang
Universität Regensburg
34 PUBLICATIONS **1,094** CITATIONS
SEE PROFILE

NANO LETTERS

pubs.acs.org/NanoLett

Resolving Single-Molecule Assembled Patterns with Superresolution Blink-Microscopy

Thorben Cordes,† Mathias Strackharn,† Stefan W. Stahl, Wolfram Summerer, Christian Steinhauer, Carsten Forthmann, Elias M. Puchner, Jan Vogelsang, Hermann E. Gaub, and Philip Tinnefeld*

Applied Physics—Biophysics and Center for NanoScience, Ludwig-Maximilians-Universität, Amalienstrasse 54, D-80799 München, Germany

ABSTRACT In this paper we experimentally combine a recently developed AFM-based molecule-by-molecule assembly (single-molecule cut-and-paste, SMCP) with subdiffraction resolution fluorescence imaging. Using "Blink-Microscopy", which exploits the fluctuating emission of single molecules for the reconstruction of superresolution images, we resolved SMCP assembled structures with features below the diffraction limit. Artificial line patterns then served as calibration structures to characterize parameters, such as the labeling density, that can influence resolution of Blink-Microscopy besides the localization precision of a single molecule. Finally, we experimentally utilized the adjustability of blink parameters to demonstrate the general connection of photophysical parameters with spatial resolution and acquisition time in superresolution microscopy.

KEYWORDS Superresolution microscopy, single-molecule cut-and-paste, superresolution calibration, single-molecule fluorescence, blink-microscopy, atomic force microscope (AFM)

Modern fluorescence microscopy techniques localize the position of individual molecules with nanometer precision,[1] and by temporally separating the fluorescence of the emitters allow subdiffraction resolution imaging of complex samples such as biological specimen.[2−7] The so-called Blink-Microscopy belongs to this class of techniques[7] that can find a broad range of novel applications in cell biology as well as material sciences. This in turn has raised fundamental questions on the interplay between fluorophore density and achievable resolution as a function of the specific parameters of the method and the fluorescent probes used.

A thorough validation of novel superresolution microscopy techniques requires well-defined samples with programmable positions of individual fluorophores. Prominent examples for bottom-up approaches to assemble such structures are DNA-origami,[8,9] dip-pen nanolithography,[10] nanopipette deposition,[11] or a "one-by-one" assembly, for example, single-molecule cut-and-paste (SMCP) surface assembly.[12−14] In this paper, we combine SMCP surface assembly with superresolution microscopy based on the subsequent localization of single fluorophores termed Blink-Microscopy. We used SMCP to create structures with subwavelength size features and used Blink-Microscopy to resolve these structures. We then assembled calibration patterns by SMCP and used them to clarify questions regarding blink parameters, achievable resolution, and maximal resolvable fluorophore density. In particular, we experimentally demonstrate the trade-off between spatial resolution and acquisition time of Blink-Microscopy and related approaches.[7,15,16]

SMCP is based on the bottom-up assembly of DNA-oligomers and offers a spatial precision down to a few nanometers for placing single molecules (see Figure 1a,b).[13] The units to be assembled, here fluorophore-labeled DNA, are picked up with an AFM tip from a depot and transferred to a target area (Figure 1, see Supporting Information, Material and Methods for details). The directionality of the process is provided by a hierarchical force system and the selectivity of DNA hybridization. The bond of the transfer DNA to the DNA immobilized at the cantilever tip is stronger than the one to the DNA in the depot area. DNA immobilized in the target area, finally, is mechanically most stable. As this process may be repeated several thousand times with the same AFM tip, SMCP allows the assembly of arbitrary structures in two dimensions. Since the small molecules are often assembled on soft surfaces, it is difficult to resolve the structures from their topology. Previous attempts to monitor the positions of molecules placed at subwavelength distances were limited to only a few single molecules.[13]

On the other hand, superresolution fluorescence microscopy has tremendously evolved over the last years starting out with stimulated emission depletion (STED) microscopy.[17,18] More recent techniques are based on the subsequent localization of single molecules and utilize the fact that the position of a single emitter, detected in a wide-field microscope, can be determined with nanometer precision. To this end the fluores-

* To whom correspondence should be addressed. E-mail: philip.tinnefeld@lmu.de. Fax: +49 89 2180 2005.

†These authors contributed equally to this work.

Received for review: 11/8/2009
Published on Web: 12/17/2009

DOI: 10.1021/nl903730r | *Nano Lett.* **2010,** *10,* 645-651

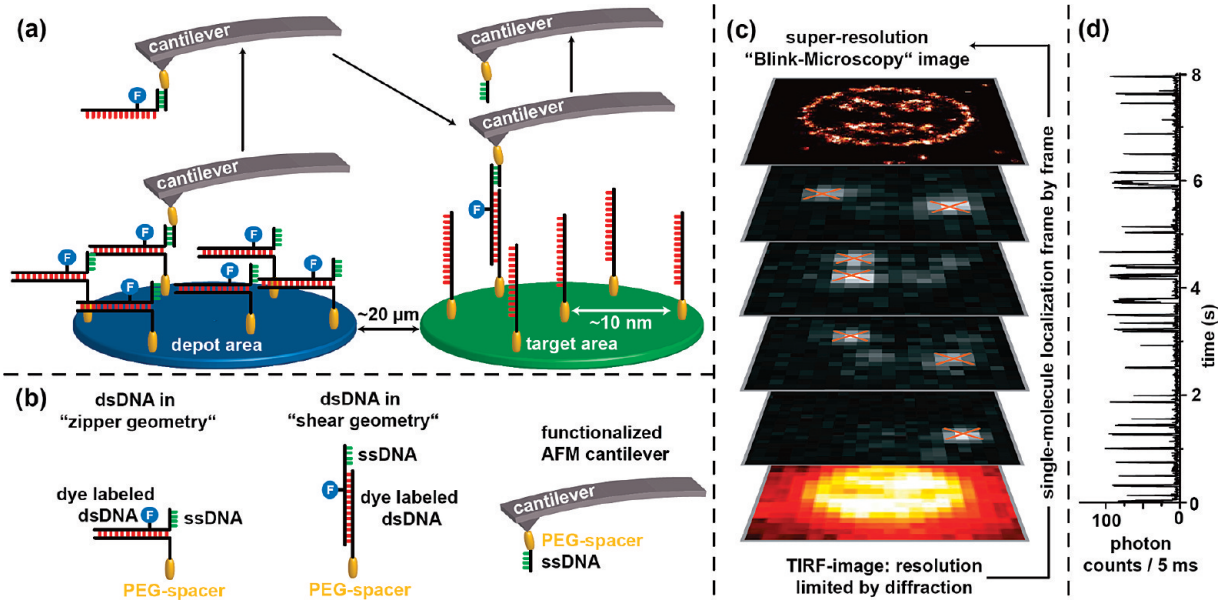

FIGURE 1. (a) Schematic illustration of single-molecule cut-and-paste and (b) corresponding caption. (c) Illustration of superresolution microscopy based on the subsequent localization of "blinking" fluorophores. (d) Fluorescent transient of a single immobilized ATTO655 molecule in aqueous PBS-buffer obtained by confocal microscopy (addition of 50 μM ascorbic acid in the presence of oxygen, excitation at 640 nm with 4 kW/cm^2).

cence of the molecules within the area of one point-spread-function is separated in time by switching all except one molecule into a nonfluorescent dark state (Figure 1c). This switching is achieved, for example, using photoswitchable fluorophores (PALM, STORM, FPALM, dSTORM)[3−6,19,20] or generic metastable dark states of the fluorophores such as radical ion states (Blink-Microscopy, GSDIM).[7,16,21−23] In Blink-Microscopy, for example, continuous ON/OFF-switching of the fluorophores is controlled by electron-transfer reactions. The environment of the fluorophore provides reductant molecules that induce the formation of radical anion states with a lifetime of nanoseconds to minutes.[7,16,24] The lifetime of these metastable OFF-states can be controlled by the oxidant concentration that restores the fluorophore in the fluorescent singlet manifold. The number of counts per cycle (ON-counts) is controlled by the reductant concentration and the ON-time is additionally adjusted by varying the excitation intensity. Blinking in single-molecule fluorescence transients reflects this redox cycle (Figure 1d).[16] Figure 1c illustrates the process of reconstructing superresolution images from movies of blinking molecules in which each single molecule is localized using a Gaussian fit.

For techniques that rely on the subsequent localization of single molecules, resolution is not clearly defined and a thorough characterization has not been performed due to the lack of calibration structures. The main factor in terms of resolution is the localization precision of single molecules, which is closely related to the number of photons detected per ON-state and the signal-to-noise ratio.[25] However, other factors that have not yet been included in a formula contribute to the achievable resolution of superresolution techniques such as the label size, the molecular and labeling density (e.g., the Nyquist criterion has to be met),[15] and the fraction of molecules that are actually (photo)activated and not photobleached. In addition, for techniques with spontaneous formation of the fluorescent form, the ratio of OFF- to ON-times (τ_{off}/τ_{on}) limits the number of fluorophores that can actually be colocalized within one diffraction limited area.[7] While this limitation obviously applies to Blink-Microscopy and related realizations of superresolution microscopy,[7,21−23] it is also important for techniques that apply photochromic molecules due to common spontaneous activation of, for example, fluorescent proteins and cyanine dyes or in case of the two wavelengths for switching and readout are used simultaneously.[26] Hitherto, the resolving power of superresolution microscopy has commonly been demonstrated with comparably undefined filamentous proteins such as actins and microtubules that were stained in vitro or in fixed cells. Test and calibration systems are required that have a defined structure with a known number of fluorophores to quantify the factors influencing resolution and to make the different techniques comparable with each other.

Recently, the use of dye-labeled DNA-origami as a nanoscopic distance ruler serving as a calibration standard for superresolution microscopy was established.[9] Here, two fluorophores with designed distance were suggested for calibrating superresolution microscopes. In contrast to this work, we now created structures by the complementary SMCP approach to demonstrate that complex structures, which are not resolvable by conventional microscopy, can be resolved utilizing Blink-Microscopy. In detail, the flexibility of SMCP was used to assemble complex structures with more than a hundred fluorophores that served for a characterization of parameters that influence resolution of

DOI: 10.1021/nl903730r | *Nano Lett.* **2010,** *10,* 645-651

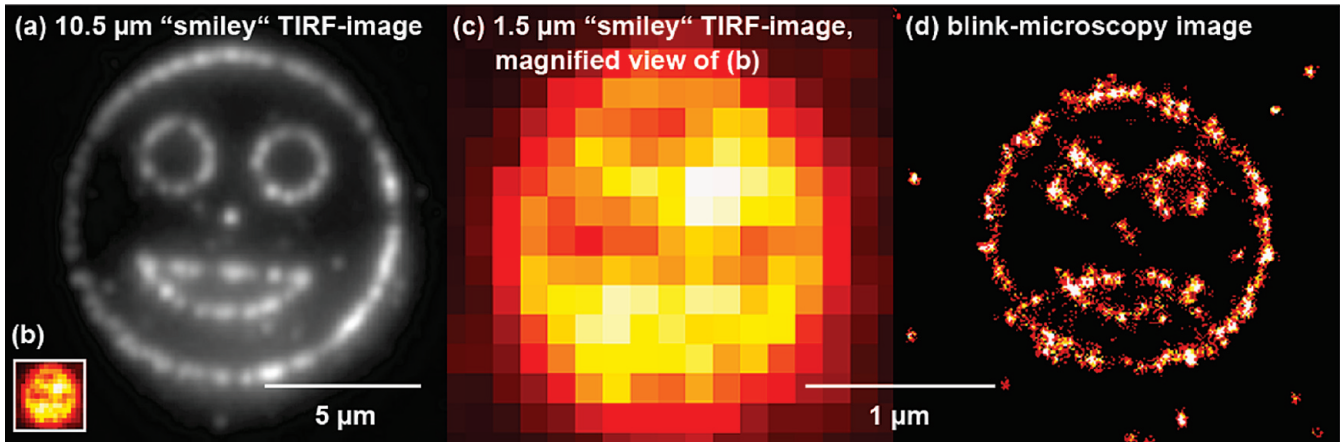

FIGURE 2. Images of patterns assembled by single-molecule cut-and-paste. (a) TIRF-image of a 10.5 μm diameter smiley (~650 transport-DNA labeled with the fluorophore Cy3; experiment conducted in PBS-buffer, 532 nm excitation with ~0.25 kW/cm^2) and (b) TIRF image of a 1.5 μm diameter smiley from another experiment as inset (~125 transported DNA labeled with the fluorophore ATTO655; experiment conducted in PBS-buffer, 50 μM AA as reductant, ambient oxygen as oxidant, 647 nm excitation with ~ 50 kW/cm^2). Scale bar for both panels (a,b) is 5 μm. (c,d) Magnified TIRF image and corresponding superresolution image of the smiley from inset panel (b) with 1.5 μm diameter; please note the smaller size of the scale bar of 1 μm corresponding to panels (c,d).

Blink-Microscopy. For example, line patterns were created to characterize the trade-off between spatial and temporal resolution of superresolution methods that separate the fluorophore emission of single emitters in time.

First, we assembled structures such as a smiley and visualized the patterns with fluorescence microscopy. Figure 2a shows an image of a smiley structure with a diameter of 10.5 μm. For this image an approximate number of 650 DNA-oligomers and attached Cy3-fluorophores were transported. All details of the structure, for example, eyes, nose, and mouth could be clearly resolved utilizing total-internal-reflection fluorescence (TIRF) microscopy.

In another experiment with the dye ATTO655 we reduced the size of the assembled smiley by a factor of ~7 down to 1.5 μm diameter, resulting in a structure with subwavelength size features. In contrast to the data in Figure 2a, no details of this smiley (Figure 2b, inset), except its circular structure, could be resolved (Figure 2b,c). Subdiffraction resolution images were subsequently recorded utilizing Blink-Microscopy. For recording these images, the oxazine dye ATTO655 was used in combination with 50 μM ascorbic acid (AA) in the presence of oxygen. Under these conditions, ATTO655 showed continuous blinking (see Figure 1d and ref 16) allowing a superresolution image to be obtained. Figure 2d clearly reveals all details of the smiley with eyes, nose, and mouth. A few gaps in the image are related to a significant fraction of inactive molecules among the transported fluorophores. In contrast to Cy3, we found that a fraction of ATTO655 fluorophores degraded during a drying step of the surface preparation procedure (see Supporting Information for details on sample preparation). The data presented in Figure 2 already demonstrates that Blink-Microscopy is a valuable tool for studying the nanomechanical assembly of SMCP on a length-scale below 200 nm.

Next, SMCP was utilized for a quantitative characterization of parameters that determine resolution for Blink-Microscopy and related approaches.[21,22] For isolated single immobilized ATTO655, that is, molecules which are not located in a distinct pattern (see points in Figures 2 and 3), OFF-times were determined to $\tau_{off} = 430$ ms, ON-times were ~2−3 ms with 800 ± 400 ON-counts under the applied buffer conditions (aerated PBS with 50 μM AA; for further details see Supporting Information). Those single molecules could be localized with a precision of 20 ± 4 nm, in accordance with theoretical expectations (a discussion of the experimentally observed versus theoretically expected resolution is found in the Supporting Information and ref 27).

When assembling line-structures with SMCP (Figure 3), we found an experimental width of a single line of 56 ± 16 nm. This value was derived from ~40 lines with 500 nm length, where each line consisted of several ATTO655 fluorophores assembled at 15 nm separation. The standard deviations were determined from Gaussian fits of a projection of the localization frequency at a single coordinate onto the x-axis, which results in histograms such as depicted in Figure 3c,j. This larger line width of 56 nm compared to the localization precision of single molecules of 20 nm is related to noise of the SMCP process. With a nominal tip diameter of ~20 nm and a flexible polymer handle that induces an uncertainty of ±10 nm,[13] we estimated the spatial accuracy of SMCP, which is directly related to the physical width of the assembled line to 40 nm. The SMCP-precision was caused by a denser functionalization of the cantilever compared to previous experiments.[13] Together with the optical localization precision of Blink-Microscopy of 20 nm, the expected measured line width by Blink-Microscopy was of the order of ~60 nm, a value that is in neat accordance with the experimentally determined width of a single line of 56 ± 16 nm.

DOI: 10.1021/nl903730r | *Nano Lett.* **2010,** *10,* 645-651

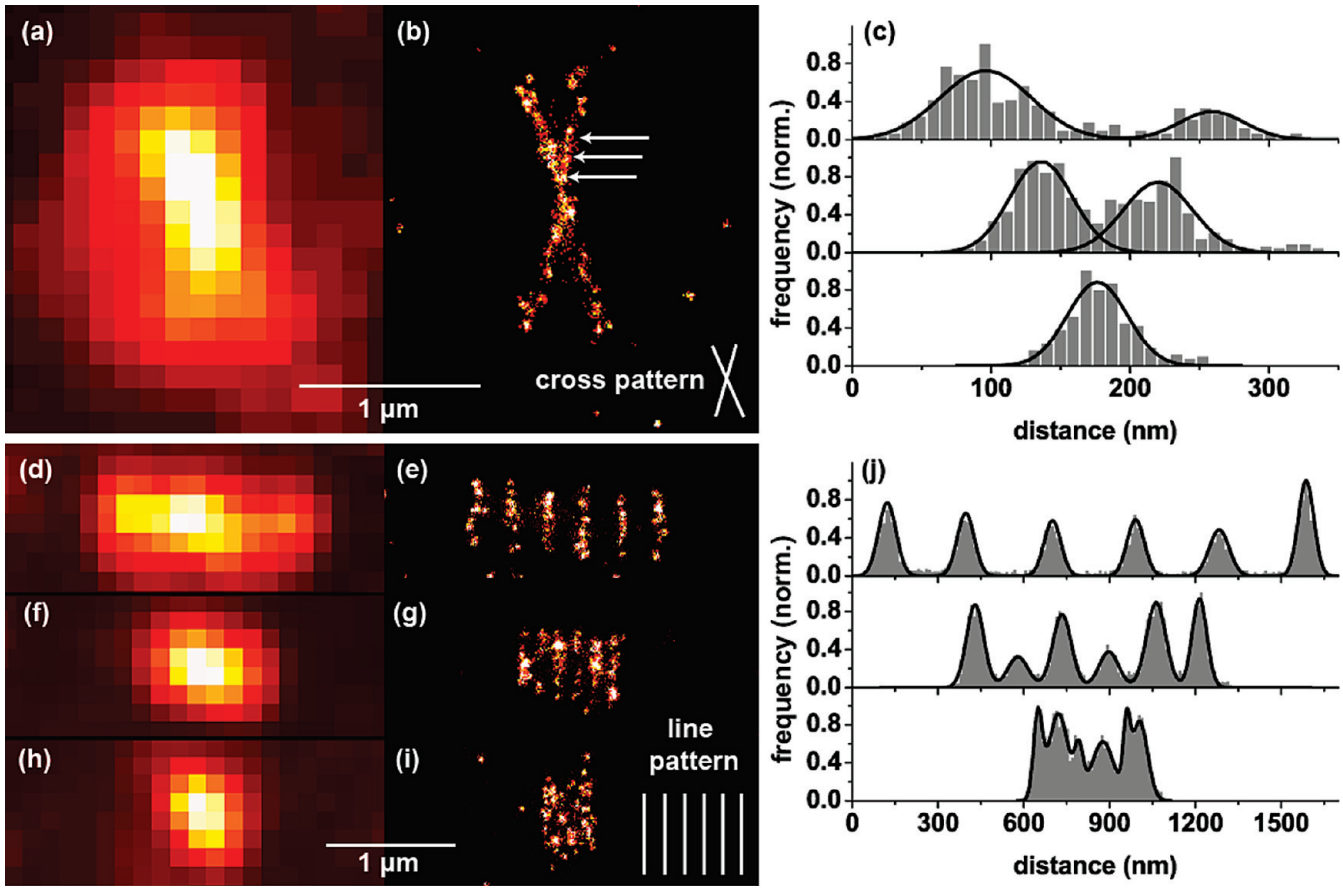

FIGURE 3. Examples of Blink-Microscopy images of subdiffraction patterns assembled by SMCP (PBS containing 50 μM AA as reductant, ambient oxygen served as oxidant). (a,b) TIRF and superresolution image of a cross pattern consisting of two lines (1.5 μm length) intersecting at an angle of 35°. The cross pattern consists of ~180 fluorophores. Panel (c) shows the corresponding histograms of single-molecule localizations at marked positions, at the positions indicated in panel (b). These histograms show that line distances of 160 nm (upper panel) and 80 nm (middle part) were clearly resolved, whereas in the range of the line-width (50 nm, lower part) the lines were no longer distinguishable. (d−i) Line grids consisting of a pattern of six parallel lines (0.5 μm length, representing ~150 active fluorophores) with decreasing spacing between the lines. Panels (d,e) show a TIRF and a superresolution image of a line grid with 300 nm spacing, (f,g) show data for 150 nm spacing, and (h,i) show data of a line grid with 75 nm spacing. Corresponding histograms of single-molecule localizations for the different superresolution images of the line grids are displayed in panel (j).

The combination of SMCP and Blink-Microscopy was then used for an actual calibration and characterization of (i) spatial resolution and (ii) resolvable fluorophore density. Therefore two different types of calibration structures were assembled with ATTO655 labeled DNA and subsequently imaged with superresolution microscopy to resolve the assembled structure. Figure 3 shows the TIRF (a) and corresponding superresolution image (b) of a "cross pattern" consisting of two lines with 1.5 μm length, intersecting at an angle of 35°. The superresolution image (Figure 3b) clearly reveals the fine-structure of the cross pattern that is not resolved in the TIRF-image (Figure 3a). The cross pattern was analyzed by taking horizontal slices of single-molecule localizations as shown in Figure 3c. Arrows in Figure 3b mark the different positions where histograms were taken. The depicted histograms were generated by a projection of the absolute number of single-molecule localizations of the respective pixel onto the horizontal axis. Histograms at the different positions reveal that a peak to peak distance of 160 nm (Figure 3c, upper panel) and 80 nm (Figure 3c, middle panel) between the lines was easily resolved. The histogram corresponding to the lowest arrow (Figure 3c, lower panel) in Figure 3b shows that in the range of the line-width of ~50−60 nm the two lines are no longer distinguishable. These data show that the achievable resolution when assembling and imaging line patterns is in the range of ~50−60 nm due to combined errors from SMCP and Blink-Microscopy.

The cross-pattern allows a qualitative estimate of the achievable spatial resolution of SMCP assembled lines. When several lines are close together the fluorophore density within one diffraction-limited area that is within 310 nm FWHM (full width at half-maximum) in our microscope increases. This leads to an increasing probability that two fluorophores emit simultaneously and deteriorate resolution. Blink-Microscopy offers an easy way to react to higher fluorophore density since the ON-counts and OFF-times are independently tunable through variation of the concentrations of reductant and oxidant, respectively.[16] At higher

DOI: 10.1021/nl903730r | *Nano Lett.* **2010,** *10,* 645-651

oxidant concentration, the OFF-times are shortened and the number of molecules that can be independently localized decreases. The advantage, however, is the fast recording time with fast blinking since more molecules could be localized within a shorter period of time. Vice versa, the OFF-times can be extended to react to the fluorophore density of the sample and the structural details to be resolved by decreasing the oxidant concentration. The τ_{off}/τ_{on}-ratio thereby is the central parameter that determines the resolvable fluorophore density. In order to quantify this trade-off of spatial and temporal resolution experimentally,[7,15] we assembled patterns consisting of six parallel lines with a variable spacing between them. The size of the grids was always greater than the size of the PSF, so that the grid-size is effectively infinite for an observation volume in the middle of the grid. The spacing between the lines was varied between 300 and 50 nm thereby increasing the fluorophore density. Subsequently, superresolution blink-images were recorded to check whether the respective line grid could be resolved at a given ratio of τ_{off}/τ_{on}. We defined a line grid resolved, if all the lines within the structure were clearly separated, i.e., six separate peaks with the appropriate spacing were observed in the histograms. Subsequently, we varied the OFF-times using different oxidant concentrations in order to experimentally study the trade-off between spatial and temporal resolution.

Figure 3 shows three line grids with a spacing of 300 nm (Figure 3d,e and associated histogram in the upper panel of Figure 3j), 150 nm (Figure 3f,g and associated histogram in the middle panel of Figure 3j) and 75 nm (Figure 3h,i and associated histogram in the lower panel of Figure 3j). With TIRF-microscopy, none of the grids was resolved as expected for the line-spacing and pixel-size of the TIRF-image of 137 nm. The superresolution images (Figure 3e,g,h) and the associated histograms (Figure 3j, 50 μM AA in the presence of oxygen, ratio of $\tau_{off}/\tau_{on} = 200$) reveal that the grids are resolved utilizing Blink-Microscopy; all histograms show six peaks at average distances of 292 ± 12 nm for the 300 nm line grid (Figure 3j, upper panel), 157 ± 7 nm for the 150 nm line grid (Figure 3j, middle panel), and 71 ± 15 nm for the 75 nm line grid (Figure 3j, lower panel).

Next, we quantified the fluorophore density for different line grids using the following approximation. In the case of aerated PBS with 50 μM AA and no 1,1′-dimethyl-4,4′-bipyridinium dichloride hydrate (methyl viologen, MV) present, the average number of localizations for a single-molecule over 8000 frames was 35 ± 16. A typical line grid, as shown in Figure 3, was characterized by 3000−4000 localizations over 8000 frames which translates into a maximal number of ~150 active fluorophores per grid. Note that this approximation incorporates the fact that the spot-finding algorithm discards ~25% of all localized events. This means that a single line with a length of 1 μm typically consists of ~50 active fluorophores. Using this approximation, we estimated the fluorophore density in molecules per μm^2 for different line grids; a line grid with 300 nm spacing shows a density of ~150 fluorophores/μm^2, a grid of 200 nm ~250 fluorophores/μm^2, a grid of 150 nm spacing contains ~300 fluorophores/μm^2, a grid of 100 nm spacing contains ~500 fluorophores/μm^2, a grid of 75 nm spacing contains ~650 fluorophores/μm^2, and finally a 50 nm grid contains 1000 fluorophores/μm^2.

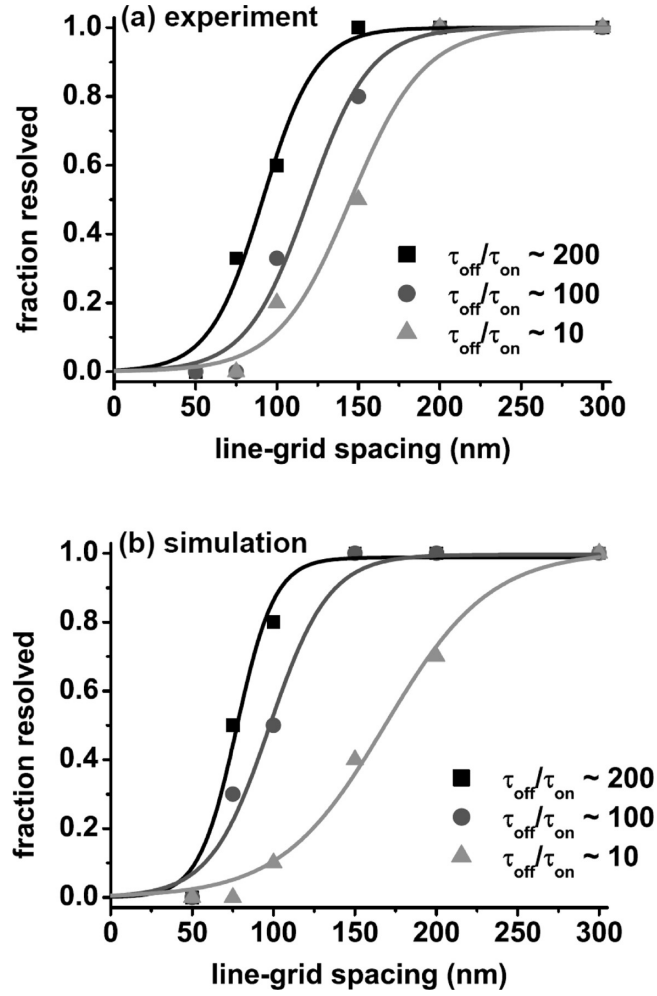

FIGURE 4. (a) Experimental values of the resolved line grid fraction for different ratios of τ_{off}/τ_{on}. The data were fitted with sigmoidal functions $y(x) = 1 - 1/(1 + e^{(x-a)/b})$ with a and b as free parameters. Further details about the statistics of the experiments and the determination of ON- and OFF-times can be found in the Supporting Information. (b) Similar results and associated fit functions of Monte Carlo-Simulations; for details, see Supporting Information.

To quantify the achievable number of resolved fluorophores per PSF-width in terms of "resolvable line grid fraction", which is the number of resolved line grids divided by the total number of measured line grids, similar experiments as depicted in Figure 3 were repeated several times. On average four line grids per spacing were analyzed (see Table S1 in Supporting Information for details). Thereby, care was taken to compare only those line grids bearing a similar number of active fluorophores. Figure 4 shows the

DOI: 10.1021/nl903730r | Nano Lett. 2010, 10, 645-651

fraction of resolved line grids for different line-spacings together with sigmoidal fits for different values of τ_{off}/τ_{on}. The reversal point indicates the line grid spacing where 50% of the line grids were resolved for a certain τ_{off}/τ_{on}-ratio.

Starting with a ratio of τ_{off}/τ_{on} ~200 (Figure 4, black; concentration of the oxidant MV = 0 μM) shows that down to a line grid spacing of 150 nm (~300 fluorophores/μm^2) all grids were resolved while significant fractions of line grids with 100 and 75 nm spacing, corresponding to ~500−650 fluorophores/μm^2, are still resolved. Grids with 50 nm spacing and a fluorophore density of 1000 fluorophores/μm^2 cannot be resolved. A sigmoidal fit reveals that a fraction of 50% is resolved at a grid-size of 91 ± 3 nm (Figure 4, black) corresponding to an estimated fluorophore density of ~530 fluorophores/μm^2. Since this value is close to the measured line-width discussed above, this resolution and also the density of fluorophores that can be resolved are mainly influenced by other parameters than the τ_{off}/τ_{on}-ratio of ~200. The resolution in our experiments was shown to be spatially limited to ~50−60 nm, which makes it impossible for us to resolve structures with 50 nm grid-size even with infinite τ_{off}/τ_{on}-ratio.

Subsequently, the same experiments were conducted at different concentrations of the oxidant MV, that is, at different τ_{off}/τ_{on}-ratios. Reducing this ratio to τ_{off}/τ_{on} ~100 by adding 10 μM MV to the buffer significantly alters the observed behavior (Figure 4, red). While the acquisition time can be reduced by the factor the ON-OFF duty cycle is reduced, only smaller fractions of the 150, 100, and 75 nm line grids were resolved and the reversal point is found at 119 ± 5 nm corresponding to an estimate of ~400 fluorophores/μm^2. This change is directly related to the lower number of fluorophores that could be colocalized at shorter OFF-times and experimentally demonstrates the trade-off of a lower spatial resolution at increased time resolution.

At a τ_{off}/τ_{on}-ratio of ~10, that is, a concentration of MV = 250 μM, the fraction of resolved grids decreases and shifts the turning point to 145 ± 6 nm corresponding to ~300 fluorophores/μm^2 in accordance with the proposed relation.

It is not trivial to access and quantify the parameters that describe this resolution change. This is because the spot finding and localization algorithm in the analysis software uses intensity thresholds, an area size- as well as a circularity-criterion for the selected spots.[7] Accordingly, the algorithm was often able to detect and discard spots when two molecules were simultaneously fluorescent within a diffraction limited area. We carried out Monte Carlo simulations to emulate the measurements and to be able to compare our measurements with expectations. Therefore 8000 video-frames of blinking dyes, which exhibit comparable emission properties as those recorded experimentally, were generated. In these simulations, molecules were placed in analogous line patterns with the SMCP precisions determined above (for details see Supporting Information). The simulated data sets were evaluated utilizing the same analyzing software as for the experimental data and yielded graphs and fit functions depicted in Figure 4b. The theoretical values where 50% of the line grids could be resolved were derived from sigmoidal fits, 77 ± 4 nm for τ_{off}/τ_{on} ~200, 98 ± 5 nm for τ_{off}/τ_{on} ~100, and 170 ± 10 nm for τ_{off}/τ_{on} ~10. These values show a slightly larger spread than the experimental values. They, however, support the idea that the resolution is limited by the physical line widths rather than the τ_{off}/τ_{on}-ratio for the smallest grids. The simulations further demonstrate that after a thorough photophysical characterization of the probes used for superresolution microscopy the imaging speed can be adapted to the desired resolution and thus be optimized to the specific problem.

In conclusion, we presented a combination of a recently established method for the bottom-up assembly of artificial structures (SMCP) and superresolution Blink-Microscopy. Superresolution microscopy served to image subdiffraction features in smiley-, cross-, and line grid-patterns created by SMCP that are difficult to characterize by other methods. Subsequently, we used patterns created by SMCP to experimentally demonstrate the trade-off of acquisition speed and spatial resolution of superresolution techniques that rely on the subsequent localization of single molecules. The adjustability of the blinking in Blink-Microscopy allowed adapting the photophysical parameters to achieve the desired spatial resolution at optimized acquisition rate. Accordingly, SMCP one-by-one assembled patterns turn out to be valuable structures for the characterization and calibration of superresolution microscopes. Simulations of the line grid structures complement the analysis and will be helpful to optimize algorithms used for single-molecule identification and localization.

Finally, this work shows the great potential of combining the complementary techniques of single-molecule assembly and superresolution microscopy. It is envisioned to create biochemical networks and enzyme cascades via SMCP whose interactions and functioning will then be accessible using superresolution fluorescence microscopy.

Acknowledgment. The authors thank Dominik Ho for stimulating discussions. This work was supported by the DFG (Inst 86/1051-1), the Volkswagen Foundation, the Biophotonics III Program of the BMBF/VDI (grant 13N9234), the Nanosystems Initiative Munich, and the Elitenetzwerk Bayern.

Supporting Information Available. Details of material and methods, sample preparation, single-molecule cut-and-paste, TIRF-microscopy and superresolution Blink-Microscopy, confocal microscopy; additional results from confocal microscopy and statistics of the resolved line grid fraction. This material is available free of charge via the Internet at http://pubs.acs.org.

REFERENCES AND NOTES

(1) Yildiz, A.; Forkey, J. N.; McKinney, S. A.; Ha, T.; Goldman, Y. E.; Selvin, P. R. *Science* **2003**, *300* (5628), 2061–2065.
(2) Hell, S. W. *Science* **2007**, *316* (5828), 1153–1158.

DOI: 10.1021/nl903730r | *Nano Lett.* **2010,** *10,* 645-651

(3) Betzig, E.; Patterson, G. H.; Sougrat, R.; Lindwasser, O. W.; Olenych, S.; Bonifacino, J. S.; Davidson, M. W.; Lippincott-Schwartz, J.; Hess, H. F. *Science* **2006**, *313* (5793), 1642–1645.
(4) Rust, M. J.; Bates, M.; Zhuang, X. *Nat. Methods* **2006**, *3* (10), 793–5.
(5) Hess, S. T.; Girirajan, T. P.; Mason, M. D. *Biophys. J.* **2006**, *91* (11), 4258–72.
(6) Heilemann, M.; van de Linde, S.; Schuttpelz, M.; Kasper, R.; Seefeldt, B.; Mukherjee, A.; Tinnefeld, P.; Sauer, M. *Angew. Chem., Int. Ed.* **2008**, *47* (33), 6172–6176.
(7) Steinhauer, C.; Forthmann, C.; Vogelsang, J.; Tinnefeld, P. *J. Am. Chem. Soc.* **2008**, *130* (50), 16840–16841.
(8) Rothemund, P. W. *Nature* **2006**, *440* (7082), 297–302.
(9) Steinhauer, C.; Jungmann, R.; Sobey, T. L.; Simmel, F. C.; Tinnefeld, P. *Angew. Chem., Int. Ed.* **2009**, *48* (47), 8870–8873.
(10) Piner, R. D.; Zhu, J.; Xu, F.; Hong, S.; Mirkin, C. A. *Science* **1999**, *283* (5402), 661–3.
(11) Rodolfa, K. T.; Bruckbauer, A.; Zhou, D. J.; Korchev, Y. E.; Klenerman, D. *Angew. Chem., Int. Ed.* **2005**, *44* (42), 6854–6859.
(12) Kufer, S. K.; Puchner, E. M.; Gumpp, H.; Liedl, T.; Gaub, H. E. *Science* **2008**, *319* (5863), 594–596.
(13) Kufer, S. K.; Strackharn, M.; Stahl, S. W.; Gumpp, H.; Puchner, E. M.; Gaub, H. E. *Nat. Nanotechnol.* **2009**, *4* (1), 45–9.
(14) Puchner, E. M.; Kufer, S. K.; Strackharn, M.; Stahl, S. W.; Gaub, H. E. *Nano Lett.* **2008**, *8* (11), 3692–5.
(15) Shroff, H.; Galbraith, C. G.; Galbraith, J. A.; Betzig, E. *Nat. Methods* **2008**, *5* (5), 417–23.
(16) Vogelsang, J.; Cordes, T.; Forthmann, C.; Steinhauer, C.; Tinnefeld, P. *Proc. Natl. Acad. Sci. U.S.A.* **2009**, *106* (20), 8107–12.
(17) Hell, S. W. *Nat. Methods* **2009**, *6* (1), 24–32.
(18) Klar, T. A.; Jakobs, S.; Dyba, M.; Egner, A.; Hell, S. W. *Proc. Natl. Acad. Sci. U.S.A.* **2000**, *97* (15), 8206–8210.
(19) Sharonov, A.; Hochstrasser, R. M. *Proc. Natl. Acad. Sci. U.S.A.* **2006**, *103* (50), 18911–18916.
(20) Lemmer, P.; Gunkel, M.; Weiland, Y.; Muller, P.; Baddeley, D.; Kaufmann, R.; Urich, A.; Eipel, H.; Amberger, R.; Hausmann, M.; Cremer, C. *J. Microsc.* **2009**, *235* (2), 163–71.
(21) Folling, J.; Bossi, M.; Bock, H.; Medda, R.; Wurm, C. A.; Hein, B.; Jakobs, S.; Eggeling, C.; Hell, S. W. *Nat. Methods* **2008**, *5* (11), 943–5.
(22) van de Linde, S.; Kasper, R.; Heilemann, M.; Sauer, M. *Appl. Phys. B* **2008**, *93* (4), 725–731.
(23) Flors, C.; Ravarani, C. N.; Dryden, D. T. *ChemPhysChem* **2009**, *10* (13), 2201−2204.
(24) Vogelsang, J.; Kasper, R.; Steinhauer, C.; Person, B.; Heilemann, M.; Sauer, M.; Tinnefeld, P. *Angew. Chem. Int. Ed.* **2008**, *47*, 5465–5469.
(25) Thompson, R. E.; Larson, D. R.; Webb, W. W. *Biophys. J.* **2002**, *82* (5), 2775–2783.
(26) Egner, A.; Geisler, C.; von Middendorff, C.; Bock, H.; Wenzel, D.; Medda, R.; Andresen, M.; Stiel, A. C.; Jakobs, S.; Eggeling, C.; Schonle, A.; Hell, S. W. *Biophys. J.* **2007**, *93* (9), 3285–90.
(27) Bossi, M.; Folling, J.; Belov, V. N.; Boyarskiy, V. P.; Medda, R.; Egner, A.; Eggeling, C.; Schonle, A.; Hell, S. W. *Nano Lett.* **2008**, *8* (8), 2463−2468.

DOI: 10.1021/nl903730r | *Nano Lett.* **2010,** *10,* 645-651

Supporting information for the manuscript

Resolving single-molecule assembled patterns with superresolution blink-microscopy

*Thorben Cordes,[1] Mathias Strackharn,[1] Stefan W. Stahl, Wolfram Summerer, Christian Steinhauer, Carsten Forthmann, Elias M. Puchner, Jan Vogelsang, Hermann E. Gaub, and Philip Tinnefeld**

Applied Physics – Biophysics & Center for NanoScience, Ludwig-Maximilians-Universität, Amalienstr. 54, D-80799 München, Germany

[1]These authors contributed equally to this work.

*Corresponding author, philip.tinnefeld@lmu.de; fax: +49 89 2180 2005

1. Material and methods

1.1. Single-molecule cut-and-paste (SMCP)

Sample-preparation: Depot and target area were prepared on circular cover slides, all details of the procedure can be found in refs. [1-3]. The slides were amino silanized and functionalized with N-hydroxy-succinimide-ester (NHS)-PEG-maleimide (M = 5000 g/mol, Rapp Polymere, Tübingen, Germany 50 mM). Subsequently, a PDMS flow chamber with two channels, connected to a peristaltic pump, was mounted on the cover slip. One channel (depot area) was rinsed for 1 h with a 10 mM solution of depot anchor oligomer while the other channel (target area) was rinsed with a 10 mM

solution of the target oligomer. Subsequently, the depot area was additionally rinsed with a 1 µM solution of transport oligomer dissolved in phosphate buffered saline (PBS) (depot oligomer: HS-5'-TTTTTTTTTAAGTAGCTATTCGAACTATAGCTTAAGGCAGTCAA-3'; transport oligomer: 5'-TTTTTGACGTCCTTAAGCTATAGTTCGAATAGCTACTTTT*TTTTTTCATCGATAAGCTTGAT ATCGAATTCCTGCAGTTTTT-3' with T* = T-ATTO655; target oligomer: 5'-AGTAGCTATTCGAACTATAGCTTAAGGACGTCTTTTTTTTTT-3'-SH). All oligomers were of HPLC grade and were synthesized by IBA (IBA, Göttingen, Germany). Thiol-modified oligomers were reduced with TCEP before coupling to PEG to generate free mercaptans. For usage in the SCMP experiment the cover slide was rinsed with PBS buffer and placed in a custom-made sample-holder.

The SMCP-setup: All SMCP experiments were performed on a custom-built AFM at room temperature in PBS buffer. Cantilevers (Veeco MSCT and Olympus BL-AC40) were covalently functionalized with NHS-PEG-maleimide (M = 5000 g/mol) and a DNA oligomer (HS-5'-TTTTTTTTTTCTGCAGGAATTCGATATCAA-3') that is able to hybridize with the transport oligomer. Spring constants of the cantilever were determined in solution by the equipartition theorem [4], with typical values of 13 pN/nm for the MSCT-C and 70 pN/nm for the BL-AC40. To transport DNA molecules, the tip and the sample were controlled in closed loop operation with a MFP-3D controller (Asylum Research, Santa Barbara, CA, USA). Software control of the SMCP process was performed in custom-made Igor Pro 5.03 (Wave Metrics).

For experiments with ATTO655 attached to the transport DNA, SMCP was performed with a cantilever with high functionalization density to transport 2-5 strands at a time. As only a fraction of 10-20% of the transported DNA-strands showed detectable emission, this was necessary to achieve a sufficient number of active fluorophores in the assembled pattern. The high number of in-active fluorophores was most likely caused by the drying process of the cover-slide within the preparation procedure and no such degradation was noticed for Cy3.

TIRF-imaging with Cy3: Imaging with transported Cy3 dyes was performed under TIRF excitation at 532 nm with at 75 mW DPSS laser (Crystalaser, Reno, USA) through an oil immersion objective (100×, NA 1.49, CFI Apochromat TIRF, Nikon, Japan). The laser was focused on the back-focal plane of the objective, the fluorescence light was filtered by a Brightline 582/75 and imaged onto a back-illuminated EMCCD camera (128x128 pixel, Andor Ixon DV-860). More details concerning all different aspects of SMCP are found in refs. [1-3].

1.2. TIRF-Imaging with ATTO655 and superresolution blink-microscopy

Fluorescence imaging was conducted on an inverted microscope (Olympus IX-71) in objective type total-internal-reflection fluorescence (TIRF) configuration. Images were collected with a back-illuminated EMCCD camera (128x128 pixel, Andor Ixon DU-860-CS0). Excitation was at 650 nm with 300 mW (single mode diode laser XTL, Toptica) and filtered by a clean-up filter (Brightline HC 650/13, AHF Analysentechnik); the beam was coupled into an oil-immersion objective (UPlanSApo 100×, NA 1.40, Olympus) using a dual-band beamsplitter (z532/658rpc, AHF, Analysentechnik). The illumination area of 600 μm^2 was approximately twice the size of the observation area of ~300 μm^2. An image magnification of ~160 fold – corresponding to a pixel size of 137 nm – was achieved by additional lenses. The fluorescent sample light was spectrally filtered by an emission filter (HQ 700/75 M, AHF Analysentechnik).

Blink-microscopy images were collected on the same setup under the following experimental conditions and without oxygen removal: 50 µM ascorbic acid (AA) were added to phosphate-buffered saline (PBS) with variable amounts, i.e. 0-250 µM, of N,N-methylviologen (MV). Under these conditions approximately N_{on} = 800 ± 400 counts were detected from a single ATTO655 molecule per on-time in the wide-field setup. According to ref. [5] the localization precision is given by ~FWHM/$(N_{on}/2)^{1/2}$ with FWHM ~310 ± 18 nm for our setup. We excluded noise arising from

background light and camera readout which suggests a theoretical localization precision of 16 nm.[6] The experimental value of 20 ± 4 nm is slightly higher – a fact that may be explained by polarization effects [7] and the internal labeling of ATTO655 to DNA. The dye molecule was separated from the PEG-linker on the surface by ~35 double-stranded base-pairs. The typical laser power for imaging was 300 mW (~50 kW/cm^2) and 4000-16000 frames were recorded at frames rates of 250-1000 Hz. The laser power was adjusted for ON-times corresponding to the integration time of the camera of ~1-4 ms.

The image reconstruction used for superresolution imaging was conducted with custom-made software as described in refs. [8]. Briefly, the first frames of the movie, typically frames 20-150, were discarded as most of the molecules were in the active state after starting laser excitation. Subsequently, the spot-finding algorithm analyses the movie frame by frame involving a lower and upper threshold. Each intensity pattern in the respective frame is then compared to its environment (commonly 7 × 7 pixels): In the case a certain contrast value (typically 2) is reached, the spot was considered for further analysis. To exclude events with two molecules being active within one diffraction limited area and to remove events when the two-dimensional Gaussian did not converge the indentified spots needed to fulfill a circularity criterion – commonly, ~25% of all events were discarded. Two-dimensional Gaussian fitting yields the position of the emitting molecule – a histogram of all molecule positions yields the superresolution image as shown in Figures 1-3 (main text).

1.3. Confocal microscopy

Fluorescent transients from single immobilized ATTO655 molecules were recorded in a home-built confocal scanning microscope. ATTO655 molecules were immobilized according to published procedures utilizing similar procedures as for SMCP-sample preparation.[1-2] Excitation at 640 nm (spectral width ~2 nm) was based on a supercontinuum laser source (SuperK Extreme, Koheras, Denmark) in combination with acousto-optical tunable filters (AOT-Fnc-VIS, AA Optoelectronic). The laser beam was coupled into an oil-immersion objective (60×, NA 1.35, UPLSAPO60X0, Olympus)

after passing a single-mode fiber, resulting in an average excitation intensity of 4 kW/cm^2. The emitted fluorescence was collected by the same objective and spatially filtered by a 50 µm pinhole. After a bandpass filter (HQ 700/75 M, AHF Analysentechnik) fluorescence was detected on an avalanche photodiode (APD, SPCM-AQR-14; Perkin Elmer).

The photophysical properties of the transport DNA from SMCP were investigated according to ref. [9]. For this purpose a constant amount of AA (50 µM) and varying amounts of MV (0-250 µM) were added to PBS-buffer. At each MV concentration ~40 single-molecule transients were recorded. Subsequently, autocorrelation analysis was employed to extract ON- and OFF-times from each single-molecule. A detailed description of the data-evaluation is found in ref. [9].

2. Results

2.1. Blinking properties of transport DNA: ATTO655

As shown in refs. [9-11] oxazine dyes show a strong dependence of their fluorescent properties on their environment (linker-structure, pH-value, oxidant- and reducer-concentration). For a determination of specific ON- and OFF-times of ATTO655 bound to the transport DNA – needed for a quantitative estimation of the resolution enhancement (see Figure 4, main text) – we recorded the blinking kinetics as shown in Figure S1. The experiments were conducted on a confocal microscope as described above. Autocorrelation analysis revealed that the addition of 50 µM AA to aerated PBS buffer leads to frequent blinking of ATTO655 with an OFF-time duration of τ_{off} = (430 ± 90) ms. As expected, the ON-counts remain constant within experimental error (data not shown) while τ_{off} reduces with increasing MV concentration (Figure S1). Further relevant OFF-times for superresolution measurements are τ_{off} = (180 ± 35) ms at 10 µM MV and τ_{off} = (14 ± 10) ms at 250 µM MV.

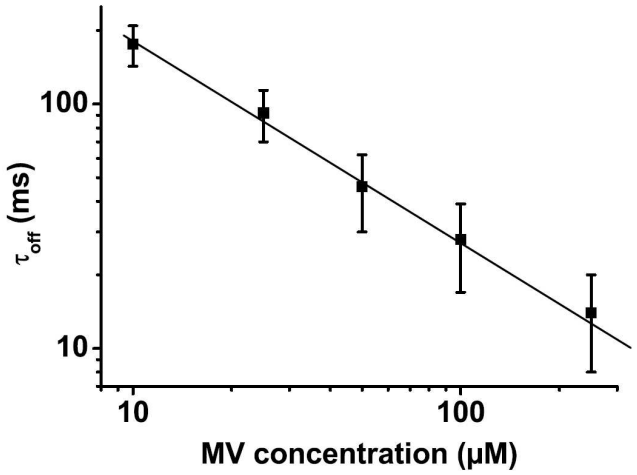

Figure S1: Double-logarithmic representation of the OFF-times of the investigated transport-DNA labeled with ATTO655 measured on a confocal microscope according to ref. [9]. For this purpose single transport DNA-strands were immobilized as described in the SCMP-section. The solid line is drawn to guide the eye.

2.2. Line grid analysis and resolved line grid fraction

In the main text an overview of the resolved line grid fraction in form of Figure 4 is given. Here, the dependence between the τ_{off}/τ_{on}-ratio and the achievable resolution, i.e., the actual number of fluorophores that can be resolved within the size of one PSF – in terms of resolved line grid fraction – is presented. Table S1 summarizes the fractions of resolved grids with respect to the numbers of measured line grids (see also Figure 4 in the main text).

Table S1: Resolved line grid fraction: actual number of resolved line grids (first number) and number of measured line grids (second number) together with the resulting resolved fraction (third number). The actual fraction is also displayed in Figure 4, main text. The values are given for a constant concentration of AA (50 µM) and varying concentrations of the oxidant MV ([MV] = 0-250 µM) for different line grid spacings (50-300 nm).

Line grid spacing	[MV] = 0 µM	[MV] = 10 µM	[MV] = 250 µM
300 nm	4 of 4; 1.0	3 of 3; 1.0	4 of 4; 1.0
200 nm	4 of 4, 1.0	3 of 3; 1.0	3 of 3; 1.0
150 nm	5 of 5; 1.0	4 of 5; 0.8	2 of 4; 0.5
100 nm	4 of 7; 0.6	3 of 6; 0.33	1 of 5; 0.2
75 nm	2 of 6; 0.33	0 of 5; 0.0	0 of 3; 0.0
50 nm	0 of 3; 0.0	0 of 3; 0.0	not determined

2.3. Monte Carlo Simulations of line grid resolved by blink-microscopy

For a detailed comparison of the experimental values from Table S1 with theory, the line grids assembled by SMCP were simulated by Monte Carlo Simulations. A description of the simulation procedure is given in ref. [8]. The simulations generated videos of 8000 frames with blinking dyes that exhibit comparable emission properties as those recorded experimentally with the EMCCD camera: ON-times were fixed to 2.5 ms with 800 ON-counts. The lines also included the experimentally determined error for the line-width and consisted of a comparable number of active fluorophores (~150). The generated videos were analyzed with the same custom-made software as described in the experimental section.

Table S2: Theoretical values of the resolved line grid fraction: actual number of resolved line grids (first number) and number of measured line grids (second number) together with the resulting resolved fraction (third number). The actual fraction is also displayed in Figure 4, main text. The values are given for a constant ON-time of 2.5 ms and varying off-time durations for different line grid spacings (50-300 nm).

Line grid spacing	τ_{off} = 400 ms	τ_{off} = 200 ms	τ_{off} = 20 ms
300 nm	5 of 5; 1.0	5 of 5; 1.0	5 of 5; 1.0
200 nm	5 of 5, 1.0	5 of 5; 1.0	7 of 10; 0.7
150 nm	5 of 5; 1.0	5 of 5; 1.0	4 of 10; 0.4
100 nm	8 of 10; 0.8	5 of 10; 0.5	1 of 10; 0.1
75 nm	5 of 10; 0.5	3 of 10; 0.3	0 of 5; 0.0
50 nm	0 of 5; 0.0	0 of 5; 0.0	0 of 5; 0.0

3. References:

1. Kufer, S.K., et al., *Single-molecule cut-and-paste surface assembly.* Science, 2008. 319(5863): p. 594-6.
2. Kufer, S.K., et al., *Optically monitoring the mechanical assembly of single molecules.* Nat Nanotechnol, 2009. 4(1): p. 45-9.
3. Puchner, E.M., et al., *Nanoparticle self-assembly on a DNA-scaffold written by single-molecule cut-and-paste.* Nano Lett, 2008. 8(11): p. 3692-5.
4. Butt, H.J. and M. Jaschke, *Calculation of thermal noise in atomic force microscopy.* Nanotechnology, 1995. 6: p. 1-7.
5. Bossi, M., et al., *Multicolor Far-Field Fluorescence Nanoscopy through Isolated Detection of Distinct Molecular Species.* Nano Letters, 2008. 8(8): p. 2463-8.
6. Thompson, R.E., D.R. Larson, and W.W. Webb, *Precise nanometer localization analysis for individual fluorescent probes.* Biophys J, 2002. 82(5): p. 2775-83.
7. Enderlein, J., E. Toprak, and P.R. Selvin, *Polarization effect on position accuracy of fluorophore localization.* Opt Express, 2006. 14(18): p. 8111-20.
8. Steinhauer, C., et al., *Superresolution microscopy on the basis of engineered dark states.* J Am

Chem Soc, 2008. 130(50): p. 16840-1.
9. Vogelsang, J., et al., *Controlling the fluorescence of ordinary oxazine dyes for single-molecule switching and superresolution microscopy.* Proc Natl Acad Sci U S A, 2009. 106(20): p. 8107-12.
10. Vogelsang, J., T. Cordes, and P. Tinnefeld, *Single-molecule photophysics of oxazines on DNA and its application in a FRET switch.* Photochem Photobiol Sci, 2009. 8(4): p. 486-96.
11. Vogelsang, J., et al., *A reducing and oxidizing system minimizes photobleaching and blinking of fluorescent dyes.* Angew Chem Int Ed Engl, 2008. 47(29): p. 5465-9.